Axisymmetric solid-of-revolution finite elements with rotational degrees of freedom

Craig S. Long *, Philip W. Loveday, and Albert A. Groenwold

Abstract

Two new solid-of-revolution axisymmetric finite elements which account for hoop fibre rotations, are introduced. The first is based on an irreducible formulation, with only displacement and rotation fields assumed independently. The second element, based on a Hellinger-Reissner like formulation, possesses an additional assumed stress field. Furthermore, an element correction, often employed in membrane elements with drilling degrees of freedom to alleviate membrane-bending locking, is adapted to the axisymmetric case. The supplemental nodal rotations introduced herein enhance modelling capability, facilitating for instance the connection between axisymmetric shell and solid models. The new elements are shown to be accurate and stable on a number of popular benchmark problems when compared with previously proposed elements. In fact, for cylinders under internal pressure analysed with a regular mesh, our mixed elements predict displacement exactly, a phenomenon known as superconvergence. The new elements are also shown to be robust and accurate on a number of bending dominated problems.

Key words: Axisymmetric, finite element, rotational degrees of freedom

1 Introduction

In recent times, flat shell finite elements with in-plane rotational (drilling) degrees of freedom have become quite popular. Apart from enrichment of the displacement field, resulting in increased element accuracy, drilling degrees of freedom allow for the modelling of, for instance, folded plates and beam-slab intersections.

* Sensor Science & Technology, CSIR Material Science & Manufacturing, Box 395, Pretoria, South Africa, 0001. Tel.: +27-12-8412498. Fax: +27-12-8413895.
Email address: clong@csir.co.za (Craig S. Long).

The motivation for developing axisymmetric elements with rotational degrees of freedom is similar. Hoop fibre rotational degrees of freedom are desirable in solid-of-revolution axisymmetric elements, to accommodate their connection to axisymmetric shell elements. Furthermore, the accuracy benefits attributed to the enhanced displacement interpolations are shown herein to be similar to the planar case.

Early obstacles in the development of finite elements with drilling degrees of freedom were largely overcome by Hughes and Brezzi [1], who presented a rigorous mathematical framework in which to formulate such elements. They proposed a modified variational principle, based on the work of Reissner [2], but with improved stability properties in the discrete form. Early finite element implementations (in Cartesian coordinates) employing the formulation of Hughes and Brezzi were presented by Hughes *et al.* [3] and Ibrahimbegovic *et al.* [4,5].

Developments in mixed/hybrid membrane finite elements have been equally important during recent years. Since the assumed stress finite element presented by Pian [6], numerous formulations have been proposed. A compilation is presented by Pian [7]. Eventually, assumed stress formulations were applied to elements with drilling degrees of freedom in a single element formulation, e.g. see Aminpour [8,9], Sze and co-workers [10,11] and Geyer and Groenwold [12].

Compared to finite element development in the Cartesian coordinate frame, advances in axisymmetric finite elements residing in a cylindrical coordinate system have been relatively slow. Besides the restrictions these elements place on the geometry and boundary conditions that can be modelled, the slower pace of development is presumably due to difficulties associated with directly extending developments in planar elements to axisymmetric elements. For example, reciprocal coordinate terms as well as stress and displacement terms appearing directly in equations of equilibrium and the strain-displacement operator, respectively, add complexities.

For the purposes of this discussion, axisymmetric finite element developments may be grouped based on the origins of their variational formulations. For example, several authors have made use of Hu-Washizu-like functionals to derive accurate elements. Of these, some of the most notable are Bachrach and Belytschko [13], who used a projection method employing Gramm-Schmidt orthogonalization, to ensure the resultant stiffness matrix requires only block-diagonal inversion, thereby reducing computational effort. Wanji and Cheung [14], after earlier efforts [15], proposed a non-conforming and a refined hybrid quadrilateral axisymmetric element. They developed a general approach for constituting non-conforming displacement functions. More recently, Kasper and Taylor [16] presented a mixed-enhanced formulation for axisymmetric

problems extending their previous works in Cartesian coordinates [17].

Other authors draw on formulations based on modified Hellinger-Reissner functionals. Examples include Tian and Pian [18] who extended the rational approach for assumed stress finite element development, proposed by Pian and Sumihara [19], to apply to axisymmetric problems. Unfortunately, as pointed out in [14], these elements do not pass the patch test. Sze and Chow [20] introduced an incompatible element, incorporating an 'inversion crime' (making use of a simplified Jacobian in the strain-displacement operator). This element was then modified using an extended Hellinger-Reissner principle, and finally simplified using the concept of free formulation [21].

Finally, various researchers have used more conventional Hellinger-Reissner principles to formulate axisymmetric elements. Zongshu [22] developed a series of 8-node axisymmetric solid elements using the traditional Hellinger-Reissner model. The assumed stress fields were chosen in global coordinates, so as to satisfy equilibrium and such that the element has proper rank and is invariant with respect to a co-coordinate system shift in the direction of the axis of radial symmetry.

Weissman and Taylor [23] introduced two elements based on the Hellinger-Reissner functional. Their elements employ the popular Pian and Sumihara interpolation, modified to obtain correct rank for the axisymmetric case. The σ_{rr}, σ_{zz} and σ_{rz} terms are interpolated in the local coordinate system while the hoop stress, $\sigma_{\theta\theta}$, is interpolated in terms of global coordinates.

Renganathan *et al.* [24] proposed a hybrid stress element with the minimum 7 $\beta-$parameters and stress interpolations in global coordinates which satisfy equilibrium as well as compatibility conditions. Most recently, Jog and Annabattula [25] presented a procedure for the development of mixed axisymmetric elements based on the Hellinger-Reissner variational principle in which stress interpolations in local coordinates are formulated based on zero-energy modes resulting from reduced integration.

The aim of this paper is to extend the existing work on planar membrane elements with drilling degrees of freedom to the torsionless axisymmetric case. Furthermore, in order to ensure that accuracy benefits are maintained in the limit of near incompressibility, we introduce a mixed (assumed stress) element accounting for rotational degrees of freedom, based on a Hellinger-Reissner-like functional.

2 Problem statement

We proceed, as in [26], by defining $\bar{\Omega}$ as a closed and bounded domain occupied by a body in three dimensional space. The interior part of $\bar{\Omega}$ is denoted by Ω and it's boundary by $\partial\Omega$, $\Omega \cup \partial\Omega = \bar{\Omega}$. The measure of Ω is V and the measure of $\partial\Omega$ is S. $\mathcal{V}$ is the vector space associated with the Euclidean point space and $\mathcal{L}$ the space of all linear applications of $\mathcal{V}$ into $\mathcal{V}$, which possesses inner product $\boldsymbol{A} \cdot \boldsymbol{B} = \mathrm{tr}(\boldsymbol{A}^t \boldsymbol{B})$, $\boldsymbol{A}, \boldsymbol{B} \in \mathcal{L}$ and $\boldsymbol{A}^t$ the transpose of $\boldsymbol{A}$ (see [26]). Reference will also be made to subsets of $\mathcal{L}$, namely $\mathcal{S}$ and $\mathcal{W}$ which contain, respectively symmetric and skew-symmetric tensors in $\mathcal{L}$.

The boundary $\partial\Omega$ is split into two parts, $\partial\Omega_u$ and $\partial\Omega_t$, such that $\partial\Omega_u \cup \partial\Omega_t = \partial\Omega$ and $\partial\Omega_u \cap \partial\Omega_t = \emptyset$. On $\partial\Omega_u$ displacements $\bar{\boldsymbol{u}}$ are prescribed, while on $\partial\Omega_t$ the traction $\bar{\boldsymbol{t}}$ is prescribed. The discussion is limited to linear elastic problems and boundary terms are omitted. Boundary conditions may, however, be incorporated in the standard manner, e.g. see [4,27–29]

In the most general case, the stress tensor, $\boldsymbol{\sigma} \in \mathcal{L}$ (which is not *a priori* assumed to be symmetric), the displacement vector field $\boldsymbol{u}$, the skew-symmetric infinitesimal rotational tensor, $\boldsymbol{\psi} \in \mathcal{W}$, and the strain tensor $\boldsymbol{\epsilon} \in \mathcal{S}$ are taken as independent variables. The variational formulation requires that the rotations $\boldsymbol{\psi}$, strains $\boldsymbol{\epsilon}$ and stresses $\boldsymbol{\sigma}$, together with the displacement generalised derivatives $\boldsymbol{\nabla u}$, belong to the space of square-integrable functions over the region Ω. The Euclidean decomposition of a second-rank tensor is used, e.g.,

$$\boldsymbol{\sigma} = \mathrm{symm}\ \boldsymbol{\sigma} + \mathrm{skew}\ \boldsymbol{\sigma}, \tag{1}$$

where

$$\mathrm{symm}\ \boldsymbol{\sigma} = \frac{1}{2}(\boldsymbol{\sigma} + \boldsymbol{\sigma}^t), \quad \text{and} \tag{2}$$

$$\mathrm{skew}\ \boldsymbol{\sigma} = \frac{1}{2}(\boldsymbol{\sigma} - \boldsymbol{\sigma}^t). \tag{3}$$

The problem under consideration is now constructed as follows: Given $\boldsymbol{f}$, the body force vector, find $\boldsymbol{u}$, $\boldsymbol{\psi}$, $\boldsymbol{\sigma}$ and $\boldsymbol{\epsilon}$ such that:

$$\mathrm{div}\ \boldsymbol{\sigma} + \boldsymbol{f} = \boldsymbol{0}, \tag{4}$$

$$\mathrm{skew}\ \boldsymbol{\sigma} = \boldsymbol{0}, \tag{5}$$

$$\boldsymbol{\psi} = \mathrm{skew}\ \boldsymbol{\nabla u}, \tag{6}$$

$$\boldsymbol{\epsilon} = \mathrm{symm}\ \boldsymbol{\nabla u}, \tag{7}$$

$$\mathrm{symm}\ \boldsymbol{\sigma} = \boldsymbol{c}\ \boldsymbol{\epsilon}, \tag{8}$$

for all $\boldsymbol{x} \in \Omega$, and where $\boldsymbol{c}$ is the elasticity tensor. Equations (4) through (8) are, respectively, the linear and angular momentum balance equations, the definition of rotation in terms of displacement gradients, the compatibility

condition for strain in terms of displacement gradient and the constitutive equations.

Now, assuming a cylindrical coordinate system, the strain tensor contains the terms

$$\epsilon_{rr} = \frac{\partial u_r}{\partial r}, \qquad \epsilon_{r\theta} = \frac{1}{2}\left(\frac{1}{r}\frac{\partial u_r}{\partial \theta} + \frac{\partial u_\theta}{\partial r} - \frac{u_\theta}{r}\right), \tag{9}$$

$$\epsilon_{\theta\theta} = \frac{1}{r}\frac{\partial u_\theta}{\partial \theta} + \frac{u_r}{r}, \qquad \epsilon_{rz} = \frac{1}{2}\left(\frac{\partial u_z}{\partial r} + \frac{\partial u_r}{\partial z}\right), \tag{10}$$

$$\epsilon_{zz} = \frac{\partial u_z}{\partial z}, \qquad \epsilon_{\theta z} = \frac{1}{2}\left(\frac{\partial u_\theta}{\partial z} + \frac{1}{r}\frac{\partial u_z}{\partial \theta}\right), \tag{11}$$

and the components of rotations are defined from continuum mechanics considerations as

$$\psi_{\theta r} = \frac{1}{2r}\left(\frac{\partial (r u_\theta)}{\partial r} - \frac{\partial u_r}{\partial \theta}\right), \quad \psi_{rz} = \frac{1}{2}\left(\frac{\partial u_r}{\partial z} - \frac{\partial u_z}{\partial r}\right), \text{ and } \quad \psi_{z\theta} = \frac{1}{2}\left(\frac{1}{r}\frac{\partial u_z}{\partial \theta} - \frac{\partial u_\theta}{\partial z}\right). \tag{12}$$

However, assuming torsionless axisymmetry, these relations simplify to:

$$\epsilon_{rr} = \frac{\partial u_r}{\partial r}, \qquad \epsilon_{r\theta} = 0, \tag{13}$$

$$\epsilon_{\theta\theta} = \frac{u_r}{r}, \qquad \epsilon_{rz} = \frac{1}{2}\left(\frac{\partial u_z}{\partial r} + \frac{\partial u_r}{\partial z}\right), \tag{14}$$

$$\epsilon_{zz} = \frac{\partial u_z}{\partial z}, \qquad \epsilon_{\theta z} = 0, \tag{15}$$

and

$$\psi_{\theta r} = 0, \qquad \psi_{rz} = \frac{1}{2}\left(\frac{\partial u_r}{\partial z} - \frac{\partial u_z}{\partial r}\right), \text{ and } \qquad \psi_{z\theta} = 0. \tag{16}$$

In the sections to follow, this problem will be embodied in an irreducible finite element formulation, which requires only independent displacement and rotation fields. A second element, based on an assumed stress Hellinger-Reissner-like formulation, will also be presented.

3 Irreducible element with rotational degrees of freedom

In this section, an irreducible element with rotational degrees of freedom is introduced. Here, the term 'irreducible' refers to a formulation with the minimum number of indepedent assumed fields, i.e. u_r, u_z and ψ_{rz} which adequately

embodies equations (4) to (8) [1]. The resulting elements have three degrees of freedom per node, namely two displacements, u_r and u_z, and a rotational degree of freedom, ψ_{rz}, representing a fibre hoop rotation tangent to the fibre.

Details of the variational formulation of elements with rotational degrees of freedom are not repeated in this paper, since a more thorough discussion can be found in the references presented in Section 1. Instead, only the functionals from which the elements are derived, are presented here.

3.1 Variational formulation

The irreducible functional with only kinematic independent variables can be written as

$$\pi(\boldsymbol{u},\boldsymbol{\psi}) = \frac{1}{2}\int_\Omega \boldsymbol{c}\,\mathrm{symm}\,\boldsymbol{\nabla u}\cdot\mathrm{symm}\,\boldsymbol{\nabla u}\,\mathrm{d}V + \frac{\gamma}{2}\int_\Omega |\mathrm{skew}\,\boldsymbol{\nabla u}-\boldsymbol{\psi}|^2\,\mathrm{d}V - \int_\Omega \boldsymbol{f}\cdot\boldsymbol{u}\,\mathrm{d}V + \text{Boundary Terms.} \quad (17)$$

The variational equations arising from π can be shown to be

$$0 = \delta\pi = \int_\Omega \boldsymbol{c}\,\mathrm{symm}\,\boldsymbol{\nabla u}\cdot\mathrm{symm}\,\boldsymbol{\nabla}\delta\boldsymbol{u}\,\mathrm{d}V + \gamma\int_\Omega(\mathrm{skew}\,\boldsymbol{\nabla u}-\boldsymbol{\psi})\cdot(\mathrm{skew}\,\boldsymbol{\nabla}\delta\boldsymbol{u}-\delta\boldsymbol{\psi})\,\mathrm{d}V - \int_\Omega \boldsymbol{f}\cdot\delta\boldsymbol{u}\,\mathrm{d}V + \text{Boundary Terms.} \quad (18)$$

3.2 Finite element implementation

The finite element interpolations employed in the elements arising from the variational formulations highlighted in the foregoing are presented in this section. It is required that only the independent translation and hoop rotation fields are interpolated.

Consider a 4-node quadrilateral element with degrees of freedom as depicted in Figure 1. The reference surface of the element is defined by

$$\boldsymbol{x} \;=\; \sum_{I=1}^{4} N_I(\xi,\eta)\,\boldsymbol{x}_I, \quad (19)$$

[1] Technically speaking, only u_r and u_z are required to describe this problem if skew $\boldsymbol{\sigma}$ is *a priori* assumed zero, since ψ_{rz} can be derived from the displacements. We nevertheless refer to these elements as irreducible to distinguish them from the mixed elements to follow.

where $\boldsymbol{x}$ represents coordinates (r, z) and $N_I(\xi, \eta)$ are the isoparametric shape functions [30]. The independent rotation field is interpolated as a standard bilinear field over each element

$$\psi_{rz} \;=\; \sum_{I=1}^{4} N_I(\xi,\eta)\, \psi_{rzI}. \tag{20}$$

The r–z (in-plane) elemental displacement approximation is taken as an Allman-type interpolation, similar to the development of membrane elements [5], i.e.

$$\begin{pmatrix} u_r \\ \\ u_z \end{pmatrix} \;=\; \boldsymbol{u} \;=\; \sum_{I=1}^{4} N_I(\xi,\eta)\, \boldsymbol{u}_I \;+\; \sum_{I=5}^{8} NS_I(\xi,\eta)\, \frac{l_{JK}}{8}\, (\psi_{rzK} - \psi_{rzJ})\, \boldsymbol{n}_{JK}, \tag{21}$$

where l_{JK} and $\boldsymbol{n}_{JK}$ are the length and the outward unit normal vector on the element side associated with the corner nodes J and K, and NS_I are the serendipity shape functions. Employing matrix notation we define

$$\text{symm}\, \boldsymbol{\nabla u} \;=\; \boldsymbol{B}_{1I}\, \boldsymbol{u}_I \;+\; \boldsymbol{B}_{2I}\, \psi_{rzI}, \tag{22}$$

where $\boldsymbol{u}_I$ and ψ_{rzI} are nodal values of the displacement and the rotation fields, respectively. The $\boldsymbol{B}_{1I}$ matrix in (22) has the standard form

$$\boldsymbol{B}_{1I} \;=\; \begin{bmatrix} N_{I,r} & 0 \\ \dfrac{N_I}{r} & 0 \\ 0 & N_{I,z} \\ N_{I,z} & N_{I,r} \end{bmatrix} \;;\; I = 1,2,3,4, \tag{23}$$

where, for example, $N_{I,r} = \frac{\partial N_I}{\partial r}$. The part of the displacement interpolation associated with the rotation field is defined as

$$\boldsymbol{B}_{2I} \;=\; \frac{1}{8} \begin{bmatrix} (l_{IJ}\, \cos\alpha_{IJ}\, NS_{L,r} - l_{IK}\, \cos\alpha_{IK}\, NS_{M,r}) \\ 0 \\ (l_{IJ}\, \sin\alpha_{IJ}\, NS_{L,z} - l_{IK}\, \sin\alpha_{IK}\, NS_{M,z}) \\ \left\{ \begin{array}{c} l_{IJ}\, \cos\alpha_{IJ}\, NS_{L,z} - l_{IK}\, \cos\alpha_{IK}\, NS_{M,z} \\ + \\ l_{IJ}\, \sin\alpha_{IJ}\, NS_{L,r} - l_{IK}\, \sin\alpha_{IK}\, NS_{M,r} \end{array} \right\} \end{bmatrix}. \tag{24}$$

Now considering terms associated with the skew-symmetric part of the displacement gradient, we begin by denoting

$$\text{skew}\, \boldsymbol{\nabla u} - \psi_{rz} \;=\; \boldsymbol{b}_{1I}\, \boldsymbol{u}_I + b_{2I}\, \psi_{rzI}, \tag{25}$$

where

$$\boldsymbol{b}_{1I} \;=\; \left[-\frac{1}{2}N_{I,z} \;\; \frac{1}{2}N_{I,r}\right] \;;\quad I=1,2,3,4, \tag{26}$$

and

$$\begin{aligned} b_{2I} \;=\; & \left[-\frac{1}{16}(l_{IJ}\,\cos\alpha_{IJ}\,NS_{L,z}\,l_{IK}\,\cos\alpha_{IK}\,NS_{M,z})\right. \\ & \left.+\frac{1}{16}(l_{IJ}\,\sin\alpha_{IJ}\,NS_{L,r}\,l_{IK}\,\sin\alpha_{IK}\,NS_{M,r})-N_I\right] \;;\quad I=1,2,3,4. \end{aligned} \tag{27}$$

The indices J, K, L, M in (21), (24) and (27) are defined in, for example [5,31]. The foregoing definitions may now be used to construct the element stiffness matrix for the irreducible element.

3.2.1 A4R finite element based on functional π

The stiffness matrix for the element derived from (18) may be directly written as

$$\boldsymbol{K}_{A4R}\,\boldsymbol{a}=\boldsymbol{f}, \quad \text{where } \boldsymbol{a}=\left\{\begin{array}{c}\boldsymbol{u}\\ \\ \boldsymbol{\psi}_{rz}\end{array}\right\}, \text{ and with} \tag{28}$$

$$\boldsymbol{K}_{A4R}=\boldsymbol{K}+\boldsymbol{p}. \tag{29}$$

The first term in the stiffness matrix can be written explicitly as

$$\boldsymbol{K} \;=\; \int_\Omega [\boldsymbol{B}_1 \;\; \boldsymbol{B}_2]^T\,\boldsymbol{C}\,[\boldsymbol{B}_1 \;\; \boldsymbol{B}_2]\;\mathrm{d}\Omega. \tag{30}$$

Employing the interpolations for displacement (21) and rotations (20) and combining with (25) leads to

$$\boldsymbol{p} \;=\; \gamma\int_\Omega \left\{\begin{array}{c}\boldsymbol{b}_1\\ \boldsymbol{b}_2\end{array}\right\}\;[\boldsymbol{b}_1 \;\; \boldsymbol{b}_2]\;\mathrm{d}\Omega, \tag{31}$$

representing the second term in (18). The matrix $\boldsymbol{p}$ is integrated by a single point Gaussian quadrature. By integrating $\boldsymbol{K}$ using a full 9-point scheme and combining with $\boldsymbol{p}$, spurious zero energy modes are prevented. [2]

This element depends on a penalty parameter γ. Appropriate values for γ have been the topic of a number of studies [1,4,12,34,35]. A value of $\gamma=\mu$, with μ the shear modulus, is used throughout, even though this value may not necessarily be optimal.

[2] This is also true if a 5-point modified reduced integration scheme (e.g. see [32,33]) is employed.

Note that an element in which the skew-symmetric part of the stress tensor is retained has also been implemented, and results for this element are available from the first author upon request. In the interests of brevity, however, we present only the irreducible element considered above.

4 Mixed element with rotational degrees of freedom

We now present a mixed assumed stress element, accounting for nodal hoop rotations. Once again, the full variational formulation is not given, since it may be found in for instance [1,12].

4.1 Variational formulation

The Hellinger-Reissner-like functional, corresponding to the π functional, can be shown to be given by

$$\Pi(\boldsymbol{u},\boldsymbol{\psi},\operatorname{symm}\boldsymbol{\sigma}) = -\frac{1}{2}\int_\Omega \boldsymbol{s}\operatorname{symm}\boldsymbol{\sigma}\cdot\operatorname{symm}\boldsymbol{\sigma}\,\mathrm{d}V + \int_\Omega \operatorname{symm}\boldsymbol{\nabla}\boldsymbol{u}\cdot\operatorname{symm}\boldsymbol{\sigma}\,\mathrm{d}V + \frac{\gamma}{2}\int_\Omega |\operatorname{skew}\boldsymbol{\nabla}\boldsymbol{u}-\boldsymbol{\psi}|^2\,\mathrm{d}V - \int_\Omega \boldsymbol{f}\cdot\boldsymbol{u}\,\mathrm{d}V + \text{Boundary Terms}, \quad (32)$$

where $\boldsymbol{s}=\boldsymbol{c}^{-1}$. Setting the first variation of Π to zero, results in

$$\delta\Pi = 0 = -\int_\Omega \boldsymbol{s}\operatorname{symm}\boldsymbol{\sigma}\cdot\operatorname{symm}\delta\boldsymbol{\sigma}\,\mathrm{d}V + \int_\Omega \operatorname{symm}\boldsymbol{\nabla}\boldsymbol{u}\cdot\operatorname{symm}\delta\boldsymbol{\sigma}\,\mathrm{d}V + \int_\Omega \operatorname{symm}\boldsymbol{\sigma}\cdot\operatorname{symm}\boldsymbol{\nabla}\delta\boldsymbol{u}\,\mathrm{d}V + \gamma\int_\Omega(\operatorname{skew}\boldsymbol{\nabla}\boldsymbol{u}-\boldsymbol{\psi})\cdot(\operatorname{skew}\boldsymbol{\nabla}\delta\boldsymbol{u}-\delta\boldsymbol{\psi})\,\mathrm{d}V - \int_\Omega \boldsymbol{f}\cdot\delta\boldsymbol{u}\,\mathrm{d}V + \text{Boundary Terms}. \quad (33)$$

4.2 Finite element implementation

The element derived from Π requires interpolations for not only displacements and rotations, but an additional (independently) assumed symmetric stress field. Since the interpolations and operators presented in Section 3.2 remain applicable here, only the stress interpolation is considered in more detail in this section.

Practically all issues surrounding the selection of stress interpolations for mixed low-order planar elements have been resolved, and community consensus on the appropriate interpolation has essentially been reached. The sit-

uation with axisymmetric elements is very different, with a wide variety of approaches and interpolations continually being proposed.

Some authors propose interpolation in the global coordinate system [22,24], however the selection of stress fields in cylindrical coordinates is far more complex than in the case of planar or solid elements in Cartesian coordinates. Finding an interpolation that has the minimum number of stress modes, that is coordinate frame invariant and that does not result in element rank deficiencies, is already a challenge.

Additional complications are associated with equilibrium equations in cylindrical coordinates. The first is the necessity for reciprocal terms in the stress interpolation, which becomes problematic as $r \to 0$. Furthermore, as pointed out by Sze and Chow [20], radial and hoop stresses appear directly in the equilibrium equations. As a result, elements which *a priori* or *a posterior* satisfy equilibrium, demonstrate a false shear phenomenon due to coupling between constant and higher order stress components. For these reasons we opt to interpolate in a local coordinate system, as also done in for example [15,16,18,23,25].

In matrix form, the stress interpolation can be expressed in terms of element parameters $\boldsymbol{\beta}$, as

$$\text{symm } \boldsymbol{\sigma} = \text{symm } \boldsymbol{\sigma}_c + \text{symm } \boldsymbol{\sigma}_h = \boldsymbol{I}_c \boldsymbol{\beta}_c + \boldsymbol{T}\boldsymbol{P}_h \boldsymbol{\beta}_h, \tag{34}$$

where

$$[\text{symm } \boldsymbol{\sigma}]^T = [\sigma_{rr} \ \sigma_{\theta\theta} \ \sigma_{zz} \ \sigma_{rz}]. \tag{35}$$

$\boldsymbol{I}_c$ is a 4×4 identity matrix and there are 4 corresponding $\beta-$parameters in $\boldsymbol{\beta}_c$, allowing for the accommodation of constant stress states required to pass the patch test. The transformation matrix is given by

$$\boldsymbol{T} = \begin{bmatrix} (J_{11})^2 & 0 & (J_{21})^2 & 2J_{11}J_{21} \\ 0 & 1 & 0 & 0 \\ (J_{12})^2 & 0 & (J_{22})^2 & 2J_{12}J_{22} \\ J_{11}J_{12} & 0 & J_{21}J_{22} & J_{11}J_{22} + J_{12}J_{21} \end{bmatrix}, \tag{36}$$

with terms defined using the Jacobian, relating the $\xi - \eta$ and the $r - z$ coordinate systems, i.e.

$$\boldsymbol{J}(\xi, \eta) = \begin{bmatrix} J_{11} & J_{12} \\ J_{21} & J_{22} \end{bmatrix}. \tag{37}$$

Kasper and Taylor [16] proposed the use of an average Jacobian in computing the transformation matrix $\boldsymbol{T}$, but we have found the transformation based on

the expression in (36) to be adequate. Alternatively, some numerical cost may be spared by using a constant $\boldsymbol{T}$, evaluated at the element centroid.

There are now various possibilities for constructing the higher-order (non-constant) stress interpolations $\boldsymbol{P}_h$. We restrict ourselves to a single option however. Essentially, we adopt the procedure suggested by Jog and Annabattula [25], who proposed the selection of interpolation functions such that zero-energy modes (associated with reduced integrations schemes) are captured.

In their paper Sze and Ghali [11] proposed such an interpolation scheme for planar elements employing Allman shape functions. Similar to Jog and Annabattula [25], we append the interpolation of Sze and Ghali with a term to capture the mode associated with the planar rigid body rotation (a mode which contributes to strain in the axisymmetric case). Specifically, we choose

$$\boldsymbol{P}_h\boldsymbol{\beta}_h = \begin{bmatrix} \eta & 0 & 0 & 0 & \eta^2 & 0 \\ 0 & 0 & 0 & 0 & 0 & z_g \\ 0 & \xi & 0 & 0 & -\xi^2 & 0 \\ 0 & 0 & \eta & \xi & 0 & 0 \end{bmatrix} [\beta_5 \ \beta_6 \ \beta_7 \ \beta_8 \ \beta_9 \ \beta_{10}]^T, \text{ where} \tag{38}$$

$$z_g = J_{12}\xi + J_{22}\eta. \tag{39}$$

Once again, J_{12} and J_{22} could be replaced by their values at the origin of the local coordinate system. Considering z_g further, although Jog and Annabattula [25] suggest setting $z_g = J_{12}\xi + J_{22}\eta$, they report this to be similar to the interpolation used in Weissman and Taylor's degenerate stress field (DSF) element [23], in which this term is interpolated in global coordinates, i.e. $z_g = b_1\xi + b_3\eta + b_2\xi\eta$, where b_1, b_2 and b_3 represent Jacobian entries computed at ξ=η=0. For the proposed element, we have found little difference between the two methods. The results presented in Section 6 therefore use z_g as defined in (39) throughout.

There are naturally many other interpolations which could be evaluated, but in the interests of brevity, we will evaluate only the one presented here.

It is now possible to construct the stiffness matrix for the mixed element with hoop rotations using the assumed stress field proposed in the foregoing.

4.2.1 A4Rσ element based on functional Π

Developing a discrete form of (33), we get:

$$\begin{bmatrix} \boldsymbol{p} & [\boldsymbol{G}]^T \\ \boldsymbol{G} & -\boldsymbol{H} \end{bmatrix} \begin{Bmatrix} \boldsymbol{a} \\ \boldsymbol{\beta} \end{Bmatrix} = \begin{Bmatrix} \boldsymbol{f} \\ \boldsymbol{0} \end{Bmatrix}. \tag{40}$$

The matrix forms of $\boldsymbol{G}$ and $\boldsymbol{H}$ take on their standard forms, namely

$$\boldsymbol{G} = \int_\Omega [\boldsymbol{P}]^T \; [\boldsymbol{B}_1 \; \boldsymbol{B}_2] \; \mathrm{d}\Omega, \tag{41}$$

and

$$\boldsymbol{H} = \int_\Omega [\boldsymbol{P}]^T \boldsymbol{S} \boldsymbol{P} \, \mathrm{d}\Omega. \tag{42}$$

In our current implementation, a full 9-point Gauss quadrature is used to evaluate both $\boldsymbol{G}$ and $\boldsymbol{H}$, even though a modified reduced 5-point integration scheme is sufficient to suppress spurious zero energy modes. In order to write the problem in the standard force-displacement form, i.e.

$$\boldsymbol{K}_{A4R\sigma} \, \boldsymbol{a} = \boldsymbol{f}, \tag{43}$$

simplifications using static condensation on the element level are required. Specifically, the unknown β–parameters are condensed out, resulting in

$$\boldsymbol{\beta} = [\boldsymbol{H}]^{-1} \boldsymbol{G} \, \boldsymbol{a}, \tag{44}$$

and we can define

$$\boldsymbol{K}_\sigma = [\boldsymbol{G}]^T \, [\boldsymbol{H}]^{-1} \boldsymbol{G}. \tag{45}$$

Finally, the stiffness matrix becomes

$$\boldsymbol{K}_{A4R\sigma} = \boldsymbol{K}_\sigma + \boldsymbol{p}, \tag{46}$$

where $\boldsymbol{K}_\sigma$ is given by (45) and $\boldsymbol{p}$, integrated using a one-point rule, is given by (31).

5 Element strain correction

Often, *membrane* elements with in-plane rotations defined using Allman interpolations, employ a so-called 'membrane-bending locking correction' [12,31,36]. This is especially true when the membrane element is used as the in-plane component of a flat shell element. This correction is reported to alleviate undesirable interactions between membrane and (plate) bending actions [36].

The correction, introduced by Jetteur and Frey [37] and further developed by Taylor [36] modifies the strain definition in (22) as follows:

$$\bar{\boldsymbol{\epsilon}} = \boldsymbol{B}_{1I}\,\boldsymbol{u}_I + \boldsymbol{B}_{2I}\,\psi_{rzI} + \bar{\boldsymbol{\epsilon}}_0, \tag{47}$$

where $\bar{\boldsymbol{\epsilon}}_0$ is found by augmenting the potential energy functional with the statement

$$\int_\Omega \bar{\boldsymbol{\sigma}}^T \left(\boldsymbol{B}_{2I}\,\psi_{rzI} + \bar{\boldsymbol{\epsilon}}_0\right) \mathrm{d}\Omega, \tag{48}$$

with both $\bar{\boldsymbol{\sigma}}$ and $\bar{\boldsymbol{\epsilon}}_0$ being constant over the element, and thereby enforcing the statement

$$\boldsymbol{B}_{2I}\,\psi_{rzI} + \bar{\boldsymbol{\epsilon}}_0 = \boldsymbol{0}, \tag{49}$$

in a weak sense. Thus, $\bar{\boldsymbol{\epsilon}}_0$ may be shown to be

$$\bar{\boldsymbol{\epsilon}}_0 = -\frac{1}{\Omega}\int_\Omega \boldsymbol{B}_{2I}\,\mathrm{d}\Omega\;\psi_{rzI}, \tag{50}$$

which can in turn be substituted back into (47).

This correction is reminiscent of a correction to ensure satisfaction of the patch test, popular in incompatible elements, see for example [38]. The net result of the modified strain definition in (47) is that, at least in a weak sense, the contribution of higher-order components of the Allman interpolations are eliminated. As a result, to pass the patch test, although higher-order displacement interpolations are employed the consistent nodal loads are computed using only bilinear interpolations, thereby simplifying pre-processing.

If however this correction is not employed, the patch test can still be passed. However, the full Allman interpolations are required to compute the consistent nodal loads, generally resulting in associated nodal moments. Complications may however be experienced at boundaries where essential boundary conditions are specified.

The numerical results to follow report on elements both with and without the correction presented in (47).

6 Numerical results

The proposed elements are now evaluated on a number of standard test problems. Their performance is judged based on a comparative study with several existing elements, whose results are sourced from data collated by Wanji and Cheung [14]. Elements considered in the comparison include the following:

A4 : the standard four-node isoparametric axisymmetric element (see for example [27,30]),

LA1 : the quadrilateral non-conforming element proposed by Sze and Chow [20],
AQ4 : the quadrilateral non-conforming element proposed by Wu and Cheung [39],
SQ4 : the generalised hybrid element proposed by Wanji and Cheung [15],
HA1/FA1 : the hybrid stress elements proposed by Sze and Chow [20],
FSF/DSF : the mixed element proposed by Weissman and Taylor [23],
NAQ6 : the non-conforming element proposed by Wanji and Cheung [14], and
RHAQ6 : the refined non-conforming hybrid element presented by Wanji and Cheung [14].

Furthermore, the elements proposed in this paper are denoted as follow:

A4R : the irreducible 4-node axisymmetric element with rotational degrees of freedom based on functional π, and with stiffness matrix given by (29), and
A4Rσ : the 4-node axisymmetric element(s) with rotational degrees of freedom based on functional Π, with an assumed stress field, with stiffness matrix as in (46).

6.1 Eigenvalue analysis

Firstly, an eigenvalue analysis of a regular, undistorted element is carried out to confirm that the new elements possess the appropriate number of non-zero eigenvalues. Indeed, the proposed elements fulfill the requirement of displaying only a single zero eigenvalue, associated with a rigid body translation along the axis of radial symmetry.

6.2 Patch test

Next, each element is subjected to a standard patch test. The problem under consideration is similar to the patch test proposed by Wanji and Cheung [14], in which the boundary displacement is given by (in the radial direction) $u_r = 2r$, and (in the direction of the axis of radial symmetry) $u_z = 1 + 4\nu$, with ν representing Poisson's ratio and r the radial coordinate.

Figure 2 depicts the arbitrary mesh used for the patch test, slightly offset from the axis of symmetry. Our new elements pass this prescribed displacement, as well as an equivalent prescribed force, patch test. The patch test is passed for any value of $\gamma > 0$, with or without the correction highlighted in Section 5. However, as pointed out in Section 5, the appropriate consistent nodal loads should be used.

6.3 Node numbering invariance

This single element problem, proposed by Sze and Chow [20] and depicted in Figure 3, is used to assess the invariance (or lack thereof) of an element to node numbering. All four possible node numbering sequences are used to compute the displacement of point A, and the results compared. The newly proposed elements are found to be, to machine precision, invariant with respect to node numbering.

6.4 Thick walled cylinder under internal pressure

An infinitely long thick walled cylinder under internal pressure, analysed by considering a slice of unit thickness, is depicted in Figure 4. Figure 4(a) depicts a cylinder with an inner radius of 5 and a wall thickness of 5, analysed using a regular mesh, while Figure 4(b) and 4(c) represent the MacNeal-Harder test [40], employing a regular and a distorted mesh, respectively. The corresponding results are presented in Tables 1, 2 and 3.

As expected, our irreducible element does not perform as well as the assumed stress element, especially in the near incompressibility limit. In fact, apart from the added modelling capability, the irreducible A4R element does not offer significant benefits over the standard isoparametric A4 element. This is not surprising since the rotational degrees of freedom are not activated in these tests, and are in fact prescribed to be zero.

On the other hand, the assumed stress A4Rσ element performs very well when judged on either displacement or on stress prediction, and is almost completely insensitive to incompressibility effects. For both problems analysed with a regular mesh, displacement is predicted exactly, a phenomenon known as 'superconvergence' [25] which has only previously been observed with elements developed by Jog and Annabattula [25] and the DSF element of Weissman and Taylor [23].

6.5 Uniformly loaded simply supported circular plate

The next test problem is depicted in Figure 5 and represents a simply supported, uniformly loaded, circular plate of thickness t. The plate is discretized using two different meshes as depicted in Figures 5(a) and 5(b) respectively. Results for the mesh depicted in Figure 5(a) with varying distortion e, and plate thickness t are presented in Tables 4, 5 and 6, while results for the highly distorted mesh shown in Figure 5(b) are presented in Table 7.

From the results of this bending dominated problem presented in Tables 4 and 5, and for values of Poisson's ratio sufficiently lower than 0.5, it is apparent that the irreducible A4R element performs significantly better than the standard isoparametric A4 element on displacement accuracy. Stress accuracy is, however, not compared since displacement based elements are incapable of computing stress directly at the axis of symmetry due to the reciprocal term in hoop strain, from which the radial stress is partly derived.

Again, the assumed stress element (with or without the element strain correction) performs very well indeed, and exhibits little accuracy sensitivity to Poisson's ratio, even in the limit of incompressibility. The A4Rσ element also achieves favourable displacement and stress predictions when compared to results from previously published elements.

Still considering the problem depicted in Figure 5(a), Table 6 compares the element displacement accuracy for various values of element aspect ratio and distortion, while Poisson's ratio is fixed ($\nu = 0.25$). These results indicate that the strain correction presented in Section 5 significantly stiffens the A4R and the A4Rσ elements when element aspect ratio is high. However, without this (optional [3]) correction, the elements are shown to be extremely robust. In particular, the A4R element is apparently only susceptible to element aspect ratio when the elements are distorted and the aspect ratio is extreme. The A4Rσ element is shown to be extremely robust, demonstrating superior performance when compared to results for previously published elements.

It should however be emphasised that the differences between elements with and without the element strain correction only become notable when element aspect ratios are extreme. The correction therefore nevertheless has merit since it simplifies pre-processing of the element consistent nodal loads.

Finally, the results for the highly distorted mesh depicted in Figure 5(b) are presented in Table 7. Once again, the assumed stress A4Rσ element performs well when compared to previously proposed elements on both displacement and stress accuracy.

6.6 Sphere under internal pressure

The final test of element accuracy is depicted in Figure 6, and represents a thin sphere with inside radius, r_i, and outside radius, r_o, subjected to a unit internal pressure. Only the top hemisphere is modelled using 10 evenly spaced elements, thereby exploiting the problem symmetry. An analytical solution to

[3] Recall that both elements pass the patch test and have the proper rank with or without the correction.

this problem may be found in, for example, [41]. The material properties are as shown in the figure.

The normalised displacements at points A and B are summarised in Table 8 for various values of Poisson's ratio ν. For values of Poisson's ratio sufficiently lower than 0.5, the irreducible A4R element again performs very well. Once again, compared to previously published elements, our assumed stress A4Rσ element achieves excellent results.

7 Conclusions

In this paper, two new axisymmetric solid-of-revolution elements with hoop fibre rotational degrees of freedom were introduced. The primary objective for developing these elements was to enhance existing modelling capability, the additional rotational degree of freedom facilitating, for instance, the connection between axisymmetric shell and axisymmetric solid models. However, the new elements were shown to also demonstrate improved accuracy and robustness on a number of popular benchmark problems when compared to existing elements.

The first element, denoted A4R, possesses two displacement degrees of freedom per node, standard in axisymmetric elements, as well a single rotational degree of freedom accounting for hoop fibre rotations. A second element, based on a mixed assumed stress formulation, possessing the aforementioned rotational nodal degree of freedom was also proposed. This element, denoted A4Rσ, further improved element performance, especially in the near incompressibility limit.

The elements were derived from a variational framework, shown to be stable in the discrete form. Rotations are based on the continuum mechanics definition of rotation, and the stress tensor is not *a priori* assumed to be symmetric. Stress interpolations, possessing the minimum number of stress parameters, for the mixed elements were proposed.

Furthermore, an element strain correction often used in membrane elements to alleviate membrane-bending locking in flat shell elements, was adapted to the axisymmetric case. This correction effectively removes strain contributions from higher-order components of the Allman interpolation in a weak sense. The patch test was accordingly passed using the consistent nodal loads of the standard 4-node isoparametric axisymmetric element, thereby simplifying preprocessing. The correction may, however, hamper element performance when the element aspect ratio becomes very large. Nevertheless, the correction is optional since the patch test is passed even if it is omitted. The proposed

elements were evaluated with and without the correction.

The performance of the irreducible (i.e. without assumed stress) A4R element was shown to be superior to standard displacement elements, especially when used to analyse bending dominated problems. However, since the element is essentially displacement-based, it tends to lock in the near incompressibility limit. Furthermore, it is incapable of directly predicting stress at the axis of symmetry due to reciprocal coordinate terms in the strain evaluation.

On the other hand, the mixed assumed stress A4Rσ element was found to be extremely accurate and robust when compared to a number of previously proposed elements on a variety of test problems. This is especially true when the aforementioned element correction was omitted. For undistorted meshes, the element predicts the exact displacement for a cylinder under internal pressure, a phenomenon known as superconvergence. The element was also found to perform excellently on a number of other benchmark problems when compared to previously proposed elements.

References

[1] T.J.R. Hughes and F. Brezzi. On drilling degrees of freedom. *Comput. Methods Appl. Mech. Engrg.*, 72:105–121, 1989.

[2] E. Reissner. A note on variational principles in elasticity. *Int. J. Solids Struct.*, 1:93–95, 1965.

[3] T.J.R. Hughes, F. Brezzi, A. Masud, and I. Harari. Finite element with drilling degree of freedom: Theory and numerical evaluation. In R. Gruber, J. Periaux, and R.P. Shaw, editors, *Proceedings of the fifth International Symposium on Numerical Methods in Engineering*, volume 1, pages 3–17, Springer-Verlag, Berlin, 1989.

[4] A. Ibrahimbegovic, R.L. Taylor, and E.L. Wilson. A robust quadrilateral membrane finite element with drilling degrees of freedom. *Int. J. Numer. Meth. Engng.*, 30:445–457, 1990.

[5] A. Ibrahimbegovic and E.L. Wilson. A unified formulation for triangular and quadrilateral flat shell finite elements with six nodal degrees of freedom. *Comm. Appl. Num. Meth.*, 7:1–9, 1991.

[6] T.H.H. Pian. Derivation of element stiffness matrices by assumed stress distributions. *AIAA J.*, 2:1333–1336, 1964.

[7] T.H.H. Pian. State-of-the-art development of the hybrid/mixed finite element method. *Fin. Elem. Anal. Des.*, 21:5–20, 1995.

[8] M.A. Aminpour. An assumed-stress hybrid 4-node shell element with drilling degrees of freedom. *Int. J. Numer. Meth. Engng.*, 33:19–38, 1992.

[9] G. Rengarajan, M.A. Aminpour, and N.F. Knight. Improved assumed-stress hybrid shell element with drilling degrees of freedom for linear stress, buckling and free vibration analyses. *Int. J. Numer. Meth. Engng.*, 38:1917–1943, 1995.

[10] K.Y. Sze, C. Wanji, and Y.K. Cheung. An efficient quadrilateral plane element with drilling degrees of freedom using orthogonal stress modes. *Computers and Structures*, 42:695–705, 1992.

[11] K.Y. Sze and A. Ghali. Hybrid plane quadrilateral element with corner rotations. *ASCE Journal of Structural Engineering*, 119:2552–2572, 1993.

[12] S. Geyer and A.A. Groenwold. Two hybrid stress membrane finite element families with drilling rotations. *Int. J. Numer. Meth. Engng.*, 53:583–601, 2002.

[13] W.E. Bachrach and T. Belytschko. Axisymmetric elements with high coarse-mesh accuracy. *Computers and Structures*, 23:323–331, 1986.

[14] C. Wanji and Y.K. Cheung. The nonconforming element method and refined hybrid element method for axisymmetric solid. *Int. J. Numer. Meth. Engng.*, 39:2509–2529, 1996.

[15] C. Wanji and K.Y. Cheung. Axisymmetric solid elements by the generalized hybrid method. *Computers and Structures*, 27:745–752, 1987.

[16] E.P. Kasper and R.L. Taylor. Mixed-enhanced formulation for geometrically linear axisymmetric problems. *Int. J. Numer. Meth. Engng.*, 53:2061–2086, 2002.

[17] E.P. Kasper and R.L. Taylor. A mixed-enhanced strain method Part I: Geometrically linear problems. *Computers and Structures*, 75:237–250, 2000.

[18] Z. Tian and T.H.H. Pian. Axisymmetric solid elements by a rational hybrid stress method. *Computers and Structures*, 20, 1985.

[19] T.H.H. Pian and K. Sumihara. Rational approach for assumed stress finite elements. *Int. J. Numer. Meth. Engng.*, 20:1685–1695, 1984.

[20] K.Y. Sze and C.L. Chow. An incompatible element for axisymmetric structure and its modification by hybrid method. *Int. J. Numer. Meth. Engng.*, 31:385–405, 1991.

[21] P.G. Bergan. Finite elements based on energy orthogonal functions. *Int. J. Numer. Meth. Engng.*, 15:1541–1555, 1980.

[22] T. Zongshu. Axisymmetric solid-of-revolution elements based on the assumed stress hybrid model. *ACTA Mechanica Sinica*, 4:35–44, 1988.

[23] S.L. Weissman and R.L. Taylor. Four-node axisymmetric element based upon the Hellinger-Reissner functional. *Comput. Methods Appl. Mech. Engrg.*, 85:39–55, 1991.

[24] K. Renganathan, B. Nageswara Rao, and M.K. Jana. An efficient axisymmetric hybrid-stress-displacement formulation for compressible/nearly incompressible material. *International Journal of Pressure Vessel and Piping*, 77:651–667, 2000.

[25] C.S. Jog and R. Annabattula. The development of hybrid axisymmetric elements based on the Hellinger-Reissner variational principle. *Int. J. Numer. Meth. Engng.*, 65:2279–2291, 2007.

[26] G. Pimpinelli. An assumed strain quadrilateral element with drilling degrees of freedom. *Fin. Elem. Anal. Des.*, 41:267–283, 2004.

[27] K.-J. Bathe. *Finite Element Procedures.* Prentice-Hall International, Inc., Upper Saddle River, New Jersey 07458, 1996.

[28] T. Mura and T. Koya. *Variational Methods in Mechanics.* Oxford University Press, Inc., 200 Madison Avenue, New York, New York, 10016, 1992.

[29] T.J.R. Hughes. *The finite element method: Linear static and dynamic analysis.* Prentice-Hall, London, 1987.

[30] O.C. Zienkiewicz and R.L. Taylor. *The Finite Element Method*, volume I: Basic Formulation and Linear Problems. McGraw-Hill Book Company, London, 1989.

[31] A.A. Groenwold and N. Stander. An efficient 4-node 24 d.o.f. thick shell finite element with 5-point quadrature. *Engineering Computations*, 12:723–748, 1995.

[32] H.H. Dovey. *Extension of three dimensional analysis to shell structures using the finite element idealization.* Report no. UC SESM 74-2, Ph-D dissertation, University of California, Berkeley, 1974.

[33] C.S. Long and A.A. Groenwold. Reduced modified quadrature for quadratic membrane finite elements. *Int. J. Num. Meth. Eng.*, 61:837–855, 2004.

[34] T.J.R. Hughes, A. Masud, and I. Harari. Numerical assessment of some membrane elements with drilling degrees of freedom. *Computers and Structures*, 55:297–314, 1995.

[35] C.S. Long, S. Geyer, and A.A. Groenwold. A numerical study of the effect of penalty parameters for membrane elements with independent rotation fields and penalized equilibrium. *Fin. Elem. Anal. Des.*, 42:757–765, 2006.

[36] R.L. Taylor. Finite element analysis of linear shell problems. In J.R. Whiteman, editor, *The Mathematics of Finite Elements and Applications VI, MAFELAP*, pages 191–203, Academic Press Limited, London, 1987.

[37] P. Jetteur and F. Frey. A four node Marguerre element for non-linear shell analysis. *Engineering Computations*, 3:276–282, 1986.

[38] Y.Q. Huang and Q.S. Li. Four-node incompatible plane and axisymmetric elements with quadratic completeness in the physical space. *Int. J. Numer. Meth. Engng.*, 61:1603–1624, 2004.

[39] C.C. Wu and Y.K. Cheung. The patch test condition in curvilinear coordinates-formulation and application. *Science China A*, 8:385–405, 1992.

[40] R.H. MacNeal and R.L. Harder. A proposed standard set of problems to test finite element accuracy. *Fin. Elem. Anal. Des.*, 1:3–20, 1985.

[41] S.P. Timoshenko and J.N. Goodier. *Theory of Elasticity*. McGraw-Hill, third edition edition, 1970.

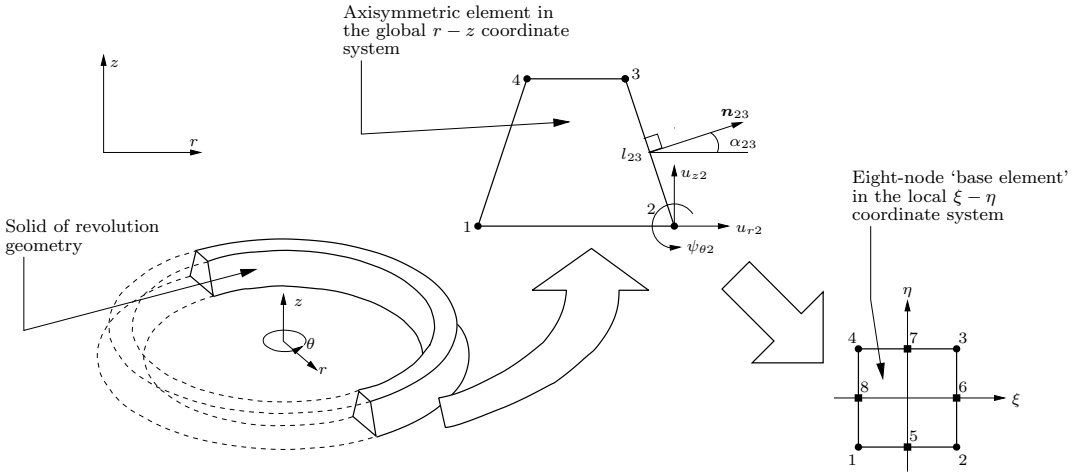

Fig. 1. Quadrilateral axisymmetric element with rotational degrees of freedom.

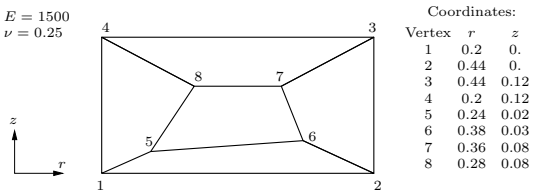

Fig. 2. Patch test geometry and material properties.

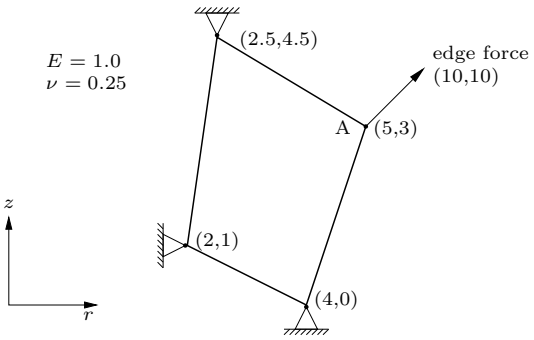

Fig. 3. Mesh used to test the sensitivity to node numbering.

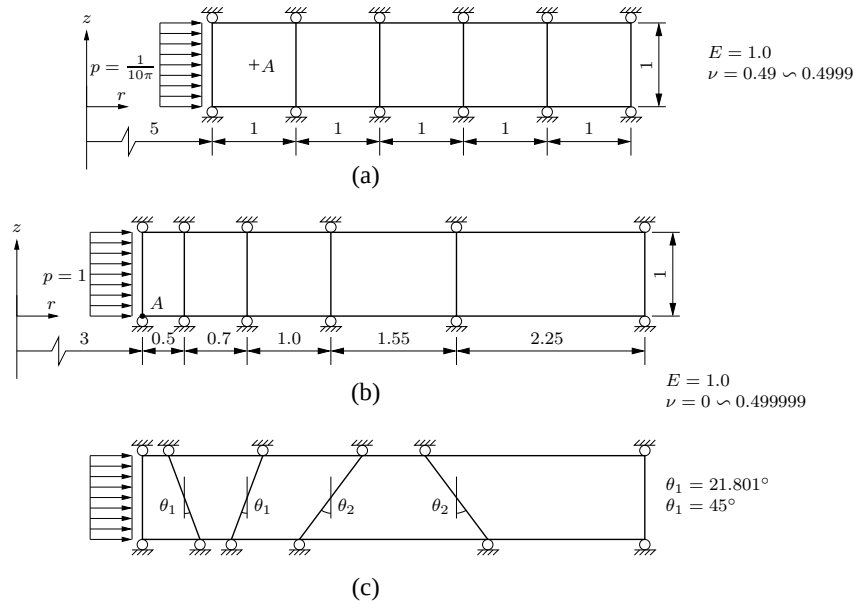

Fig. 4. Thick walled cylinder(s) under internal pressure.

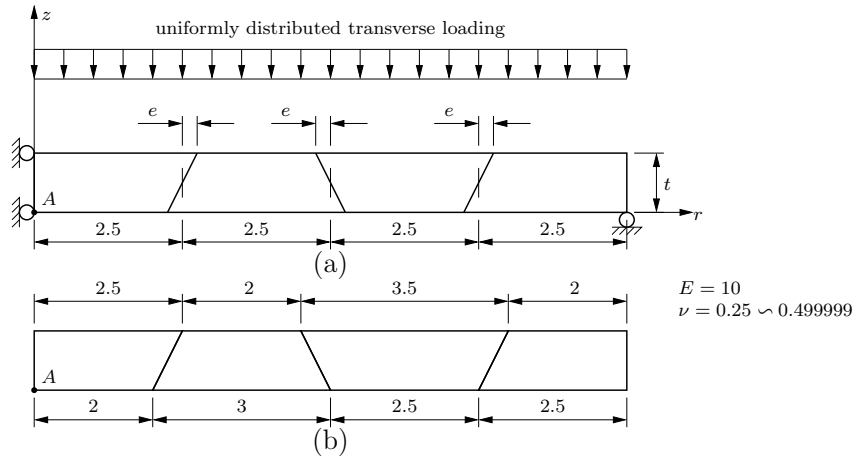

Fig. 5. Simply supported uniformly loaded circular plate.

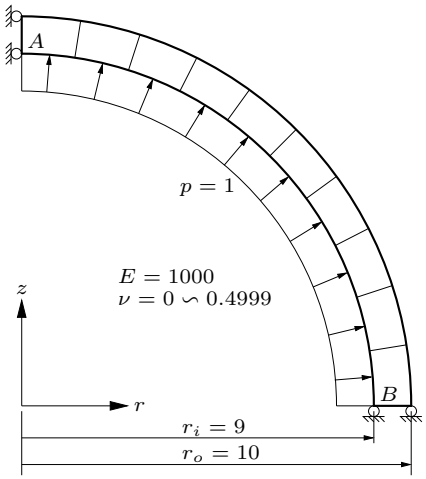

Fig. 6. Thin sphere subjected to unit internal pressure.

	$\nu = 0.49$				$\nu = 0.499$				$\nu = 0.4999$			
Element	u_r †	σ_{rA}	$\sigma_{\theta A}$	σ_{zA}	u_r †	σ_{rA}	$\sigma_{\theta A}$	σ_{zA}	u_r †	σ_{rA}	$\sigma_{\theta A}$	σ_{zA}
A4	0.906	0.817	0.963	1.129	0.494	-0.026	0.778	1.704	0.089	-0.856	0.597	2.275
LA1	0.992	-1.282	0.851	0.356	0.992	1.090	-0.584	-5.821	0.992	30.731	-14.937	-67.698
AQ6	0.992	0.996	1.011	1.029	0.992	0.996	1.011	1.028	0.992	0.996	1.011	1.028
NAQ6	0.992	0.996	1.011	1.029	0.992	0.996	1.011	1.028	0.992	0.996	1.011	1.028
SQ4	0.992	0.996	1.011	1.029	0.992	0.996	1.011	1.028	0.992	0.996	1.011	1.028
HA1/FA1	0.992	0.996	1.011	1.029	0.992	0.996	1.011	1.028	0.992	0.996	1.011	1.028
RHAQ6	0.992	0.996	1.011	1.029	0.992	0.996	1.011	1.028	0.992	0.996	1.011	1.028
A4R‡	0.906	0.817	0.963	1.130	0.494	-0.028	0.778	1.706	0.089	-0.857	0.597	2.277
A4Rσ‡	1.000	1.011	1.006	1.000	1.000	1.011	1.006	0.999	1.000	1.011	1.006	1.001
Exact	31.780	-2.450	4.570	1.040	31.830	-2.450	4.570	1.060	31.830	-2.450	4.570	1.060

† Radial displacement measured at $r = 5$.

‡ Same results with and without element strain correction.

Table 1. Normalised results for a thick-walled cylinder with regular mesh and variable Poisson's ratio (see Figure 4(a)). Exact results in 10^{-2}.

Element	$\nu = 0.0$	$\nu = 0.3$	$\nu = 0.49$	$\nu = 0.499$	$\nu = 0.4999$	$\nu = 0.499999$
A4	0.994	0.988	0.847	0.359	0.053	5.61×10^{-4}
FSF	0.994	0.990	0.986	0.986	0.986	–[†]
DSF	1.000	1.000	1.000	1.000	1.000	–[†]
AQ6	0.994	0.990	0.986	0.985	0.986	0.985
NAQ6	0.994	0.990	0.933	0.986	0.986	0.986
RHAQ6	0.994	0.990	0.986	0.986	0.986	0.986
A4R[‡]	0.994	0.988	0.846	0.358	0.053	5.59×10^{-4}
A4Rσ[‡]	1.000	1.000	1.000	1.000	1.000	1.000

[†] No results reported.

[‡] Same results with and without element strain correction.

Table 2
MacNeal-Harder test, regular mesh (see Figure 4(b)). Normalized displacement at point A.

Element	$\nu = 0.0$	$\nu = 0.3$	$\nu = 0.49$	$\nu = 0.499$	$\nu = 0.4999$	$\nu = 0.499999$
A4	0.989	0.982	0.816	0.315	0.044	4.43×10^{-4}
FSF	0.985	0.981	0.976	0.976	0.976	–[†]
DSF	0.997	0.997	0.997	0.997	0.997	–[†]
AQ6	0.991	0.985	0.938	0.718	0.472	0.410
NAQ6	0.989	0.985	0.939	0.713	0.445	0.372
RHAQ6	0.989	0.987	0.983	0.983	0.983	0.983
A4R[‡]	0.988	0.982	0.815	0.313	0.044	4.55×10^{-4}
A4Rσ[‡]	0.994	0.993	0.984	0.982	0.982	0.982

[†] No results reported.

[‡] Same results with and without element strain correction.

Table 3
MacNeal-Harder test, distorted mesh (see Figure 4(c)). Normalized displacement at point A.

Element	u_{zA}				σ_{rA}			
	$\nu = 0.25$	$\nu = 0.49$	$\nu = 0.4999$	$\nu = 0.499999$	$\nu = 0.25$	$\nu = 0.49$	$\nu = 0.4999$	$\nu = 0.499999$
A4	0.696	0.079	0.016	0.015	–†	–†	–†	–†
LA1	1.034	1.011	0.785	0.761	–†	–†	–†	–†
AQ6	1.034	1.011	0.785	0.761	0.999	0.937	0.597	0.567
NAQ6	1.034	1.011	0.785	0.761	0.999	0.936	0.596	0.566
SQ4	1.034	1.011	0.785	0.761	0.999	0.937	0.597	0.567
HA1/FA1	1.037	1.043	1.043	1.043	1.006	1.007	1.007	1.007
RHAQ6	1.037	1.043	1.043	1.043	1.006	1.008	1.008	1.008
A4R	0.868	0.080	0.016	0.015	–†	–†	–†	–†
A4R*	0.849	0.077	0.015	0.015	–†	–†	–†	–†
A4Rσ	1.014	1.011	1.010	1.010	0.952	0.939	0.936	0.936
A4Rσ*	1.004	1.009	1.009	1.009	1.000	1.000	1.000	1.000
Exact	-738.280	-524.980	-515.720	-515.630	121.880	130.880	131.250	131.250

† Not possible to compute σ_{rA} due to singularity at $r = 0$.

* Element without element strain correction.

Table 4
Normalised results for uniformly loaded circular plate with varying Poisson's ratio, modelled using a 1×4 regular mesh. See Figure 5(a), $t = 1$, $e = 0$.

Element	u_{zA}				σ_{rA}			
	$\nu = 0.25$	$\nu = 0.49$	$\nu = 0.4999$	$\nu = 0.499999$	$\nu = 0.25$	$\nu = 0.49$	$\nu = 0.4999$	$\nu = 0.499999$
A4	0.694	0.079	0.016	0.015	–†	–†	–†	–†
LA1	1.027	1.006	0.777	0.753	–†	–†	–†	–†
AQ6	1.030	1.008	0.781	0.756	1.005	0.933	0.585	0.555
NAQ6	1.030	1.008	0.781	0.757	0.980	0.879	1.344	1.329
SQ4	1.030	1.008	0.781	0.756	1.011	0.948	0.599	0.568
HA1	1.030	1.040	1.040	1.043	0.988	0.930	0.924	0.924
FA1	1.030	1.040	1.040	1.040	0.997	0.938	0.933	0.933
RHAQ6	1.030	1.041	1.041	1.041	0.994	0.998	0.998	0.998
A4R	0.865	0.080	0.016	0.015	–†	–†	–†	–†
A4R*	0.849	0.077	0.015	0.015	–†	–†	–†	–†
A4Rσ	1.009	1.008	1.007	1.007	0.971	0.956	0.953	0.953
A4Rσ*	1.004	1.009	1.009	1.009	1.003	1.003	1.003	1.003
Exact	-738.280	-524.980	-515.720	-515.630	121.880	130.880	131.250	131.250

† Not possible to compute σ_{rA} due to singularity at $r = 0$.

* Element without element strain correction.

Table 5
Normalised results for uniformly loaded circular plate with varying Poisson's ratios, modelled using a 1×4 slightly distorted mesh. See Figure 5(a), $t = 1$, $e = 0.025$.

Computed quantity	$u_{zA}t^3$ for 1×4 regular mesh			$u_{zA}t^3$ for 1×4 distorted mesh		
Element aspect ratio	2.5	100	500	2.5	100	500
A4	0.696	2.22×10^{-3}	$8.89\times^{-5}$	0.694	8.87×10^{-4}	3.84×10^{-5}
LA1	1.034	1.025	1.025	1.027	0.549	0.546
AQ6	1.034	1.025	1.025	1.030	0.493	0.491
NAQ6	1.034	1.025	1.025	1.030	0.493	0.491
SQ4	1.034	1.025	1.025	1.030	0.493	0.491
HA1	1.037	1.028	1.028	1.030	0.559	0.556
FA1	1.037	1.028	1.028	1.030	0.559	0.556
RHAQ6	1.037	1.028	1.028	1.030	0.738	0.738
A4R	0.868	0.421	0.190	0.865	5.37×10^{-3}	7.05×10^{-5}
A4R*	0.849	0.839	0.838	0.849	0.515	1.42×10^{-3}
A4Rσ	1.014	0.472	0.212	1.009	0.015	6.13×10^{-3}
A4Rσ*	1.004	0.994	0.995	1.004	0.941	0.897
Exact	-738.28					

* Element without element strain correction.

Table 6
Normalised $u_{zA}t^3$ values for various element aspect ratios ($= 2.5/t$) with $\nu = 0.25$, see Figures 5(a). Distorted mesh with $e = 0.025$.

Element	u_{zA}				σ_{rA}			
	$\nu = 0.25$	$\nu = 0.49$	$\nu = 0.4999$	$\nu = 0.499999$	$\nu = 0.25$	$\nu = 0.49$	$\nu = 0.4999$	$\nu = 0.499999$
A4	0.635	0.088	0.017	0.019	–†	–†	–†	–†
LA1	0.909	0.903	0.590	0.563	–†	–†	–†	–†
AQ6	0.907	0.906	0.593	0.566	1.389	1.132	0.370	0.328
NAQ6	0.912	0.906	0.592	0.565	1.154	0.800	3.254	3.590
SQ4	0.906	0.904	0.593	0.566	1.341	1.164	0.469	0.430
HA1	0.918	0.976	0.979	0.979	1.226	1.043	1.030	1.030
FA1	0.915	0.971	0.974	0.974	1.352	1.167	1.154	1.153
RHAQ6	0.928	0.977	0.979	0.979	0.974	1.029	1.032	1.032
A4R	0.773	0.113	0.018	0.016	–†	–†	–†	–†
A4R*	0.880	0.091	0.015	0.015	–†	–†	–†	–†
A4Rσ	0.864	0.911	0.911	0.911	1.487	1.398	1.388	1.388
A4Rσ*	0.998	1.005	1.005	1.005	1.053	1.039	1.039	1.039
Exact	-738.280	-524.980	-515.720	-515.630	121.880	130.880	131.250	131.250

† Not possible to compute σ_{rA} due to singularity at $r = 0$.

* Element without element strain correction.

Table 7
Normalised results for a uniformly loaded circular plate with varying Poisson's ratio, modelled using a 1×4 highly distorted mesh. See Figure 5(b), $t = 1$.

Element	u_{zA}					u_{rB}				
	$\nu = 0$	$\nu = 0.3$	$\nu = 0.49$	$\nu = 0.499$	$\nu = 0.4999$	$\nu = 0$	$\nu = 0.3$	$\nu = 0.49$	$\nu = 0.499$	$\nu = 0.4999$
A4	1.024	1.027	0.896	0.424	0.068	0.997	0.992	0.876	0.419	0.067
FSF	1.061	1.076	1.085	1.085	1.085	0.994	0.990	0.984	0.984	0.984
DSF	1.059	1.074	1.085	1.086	1.086	0.995	0.992	0.988	0.988	0.988
A4R	1.056	1.063	0.910	0.427	0.068	0.996	0.990	0.873	0.418	0.067
A4R*	0.999	0.995	0.883	0.421	0.068	0.998	0.993	0.878	0.420	0.069
A4Rσ	1.052	1.065	1.072	1.072	1.072	0.997	0.994	0.990	0.990	0.990
A4Rσ*	0.994	0.991	0.987	0.986	0.986	0.999	0.997	0.994	0.994	0.994
Exact	4.081	3.127	2.523	2.494	2.491	4.081	3.127	2.523	2.494	2.491

* Element without element strain correction.

Table 8
Normalised displacements for a thin sphere under internal pressure, see Figure 6. Exact solution in 10^{-2}.